JOURNAL OF GUIDANCE, CONTROL, AND DYNAMICS
Vol. 28, No. 1, January–February 2005

Adaptive Control of a Flexible Robot Using Fuzzy Logic

A. Green* and J. Z. Sasiadek†
Carleton University, Ottawa, Ontario K1S 5B6, Canada

Operational problems with robot manipulators in space relate to several factors, one most important being structural flexibility and subsequently significant difficulties with the control systems, especially for endpoint position control. Elastic vibrations of the links coupled with their large rotations and nonlinear dynamics is the primary cause. A control scheme is presented for tracking the endpoint of a two-link flexible robot. The dominant assumed modes of vibration for Euler–Bernoulli cantilever and pinned–pinned beam boundary conditions are coupled with the nonlinear dynamics for rigid links to form an Euler–Lagrange inverse flexible dynamics robot model. A Jacobian transpose control law actuating the robot joints is adapted by a fuzzy logic system (FLS) with link deformation inputs and a single-variable output. Results obtained with an FLS adaptive control strategy show significantly diminished vibration amplitudes for both cantilever and pinned–pinned link dynamics and greatly improved control performance compared to the nonadaptive strategy.

Nomenclature

$\boldsymbol{C}$	=	flexible-link dynamic coupling matrix
$\boldsymbol{C}_r$	=	rigid-link dynamic coupling matrix
EI	=	flexural rigidity, 1676 N · m^2
e_x, e_y	=	position errors, $x_c - x$ and $y_c - y$
$\dot{e}_x, \dot{e}_y$	=	velocity errors
F_i	=	generalized force, $i = 1, \ldots, n$
$\boldsymbol{J}(\theta)$	=	Jacobian of direct kinematics
$\boldsymbol{K}$	=	stiffness matrix
K_i	=	stiffness constant, $i = 1, 2$
L	=	length of each link, $L_1 = L_2 = 4.5$ m
$\mathcal{L}$	=	Lagrange function
$\boldsymbol{M}$	=	flexible-link inertia matrix
M_i	=	generalized distributed mass, $i = 1, \ldots, n$
M_{ij}	=	$[i, j]$ element of inertia tensor $\boldsymbol{M}$
$\boldsymbol{M}_r$	=	rigid-link inertia matrix
m_i	=	mass per unit length, 0.335 kg/m
$m(x)$	=	mass as a function of distance x
$p(x, t)$	=	distributed load
$\boldsymbol{q}$	=	generalized coordinates vector
q_i	=	generalized coordinates, $i = 1, \ldots, n$
T	=	total kinetic energy
T_e	=	elastic kinetic energy for flexible links
T_r	=	kinetic energy for rigid links
U	=	total potential energy
U_e	=	elastic potential energy for flexible links
U_r	=	potential energy for rigid links
$u(x, t)$	=	mode shape function
x	=	actual endpoint position
x_c	=	commanded endpoint position
y	=	actual endpoint position
y_c	=	commanded endpoint position
δ_i	=	elastic link deformation, $i = 1, 2$
ζ	=	estimated closed-loop damping ratio, 0.707
$\boldsymbol{\theta}$	=	slew angles vector
θ_t	=	link tip angle of rotation
$\dot{\boldsymbol{\theta}}$	=	slew angles velocities vector
λ	=	fuzzy logic system output variable
$\lambda_{ci}L$	=	cantilever ith mode characteristic root, $(i–0.5)\pi$
$\lambda_{ppi}L$	=	pinned–pinned ith mode characteristic root, $i\pi$
μ	=	fuzzy degree of membership
ρ	=	mass density per unit length
$\boldsymbol{\tau}$	=	actuating torque vector
ϕ_i	=	mode shape, $i = 1, \ldots, n$
ω_{ci}	=	cantilever elastic mode frequency, $i = 1, \ldots, n$
ω_i	=	elastic mode frequency, $i = 1, \ldots, n$
ω_{ppi}	=	pinned–pinned mode frequency, $i = 1, \ldots, n$

Received 9 November 2003; revision received 16 January 2004; accepted for publication 16 January 2004.

*Ph.D. Candidate, Department of Mechanical and Aerospace Engineering; agreen2@chat.carleton.ca. Senior Member AIAA.

†Professor, Department of Mechanical and Aerospace Engineering; jsas@ccs.carleton.ca. Associate Fellow AIAA.

Introduction

MINIMIZATION of vibration and precise control is a strict requirement of flexible robots in spacecraft operations. The aim of this paper is to demonstrate tracking of a square trajectory 12.6 × 12.6 m by a two-link flexible robot. The Euler–Lagrange flexible dynamics models include link flexibility based on the dominant assumed modes for Euler–Bernoulli cantilever and pinned–pinned beam boundary conditions. A square trajectory is an ideal case for studying the control of transient vibrations at the four orthogonal direction switches. Simulation studies on tracking a square trajectory for two-link rigid- and flexible-dynamics models were presented in previous work.[1–4] Excellent results were obtained using an input shaping method to reduce residual vibrations coupled with an inverse kinematics control strategy for both linear and nonlinear control laws and full-order flexible-dynamics equations based on a recursive order-n algorithm for a discretized two-link flexible robot.[1] A model reference adaptive control (MRAC) technique was applied to investigate position and vibration control of a distributed mass single-link flexible manipulator.[5] The state-space MRAC strategy used a modal expansion method to determine the first three significant vibration modes. This strategy was an attempt to achieve smaller position errors and an alternative to regular proportional–integral–derivative (PID) control that failed to give satisfactory results. An elastic potential function was derived from a modal expansion of a single flexible link with pinned–free boundary conditions and coupled with rigid-link dynamics to formulate an Euler–Lagrange dynamics manipulator model. A simple feedback control law comprising a derivative gain and velocity feedback term and a gravity compensation term was used, and PID transient responses to step and impulse inputs were compared to MRAC responses. The results demonstrate accuracy of the modal expansion method within an MRAC strategy to achieve further reduction of positioning errors and decrease settling time of transient response to step inputs.

Experimental tracking of a square trajectory by a two-link flexible space robot was performed using a series of steady-state linear regulators produced good results.[6] Also, fuzzy logic methods have been used to control robot manipulators providing various results. These

methods have involved the application of fuzzy control in various strategies. One strategy used fuzzy controllers to tune PID gains for a two-link robot with rigid links tracking a square trajectory with excellent results.[2] One used a fuzzy controller with endpoint position error and change-of-error inputs and output control variable to vary motor hub speed for a computer-simulated single-link flexible robot but with significant transient endpoint vibrations.[7] One used fuzzy controllers to vary voltage input to each motor for a two-link flexible robot in response to link accelerations and angular positions outputs also with significant transient vibrations.[8] Another strategy used two fuzzy controllers to substitute for the dynamics equations of a two-link robot tracking a square trajectory and significantly reduced endpoint transient vibrations at direction switches.[3] The purpose of the study presented in this paper is to demonstrate precision endpoint tracking by a two-link flexible robot modeled by nonlinear flexible dynamics and controlled by a fuzzy logic adaptive control strategy. The strategy is easy to construct, effective in performance, and suitable for a broad range of applications.

Two-Link Flexible Robot

The two-link flexible robot shown in Fig. 1 has planar motion and vibration modes. Gravity and friction effects are neglected for space robot applications. The robot parameters are adopted from other work.[1]

Rigid Dynamics

A conventional closed form of the nonlinear dynamics of a multilink robot with rigid links is derived in terms of kinetic and potential energies stored in the system by the Euler–Lagrange formulation (Ref. 9). Given an independent set of generalized coordinates, $q_i = q_1, \ldots, q_n$, the total kinetic and potential energies stored in the system, T and U, respectively, is defined by the Lagrangian

$$L(q_i, \dot{q}_i) = T - U, \qquad i = 1, \ldots, n \tag{1}$$

For a robot subjected to a generalized force F_i acting on a generalized coordinate q_i the dynamic equations of motion are given by

$$\frac{\mathrm{d}}{\mathrm{d}t}\frac{\partial L}{\partial \dot{q}_i} - \frac{\partial L}{\partial q_i} = F_i, \qquad i = 1, \ldots, n \tag{2}$$

Kinetic energy is given by

$$T_r = \frac{1}{2}\sum_{i=1}^{n}\sum_{j=1}^{n} M_{ij}\dot{q}_i\dot{q}_j \tag{3}$$

For space robot applications, the gravity potential energy is omitted. Hence, for an n-degree-of-freedom (n-DOF) robot the Euler–Lagrange rigid-dynamics equations are

$$\boldsymbol{\tau} = \boldsymbol{M}_r(\boldsymbol{\theta})\ddot{\boldsymbol{\theta}} + \boldsymbol{C}_r(\dot{\boldsymbol{\theta}}, \boldsymbol{\theta})\dot{\boldsymbol{\theta}} \tag{4}$$

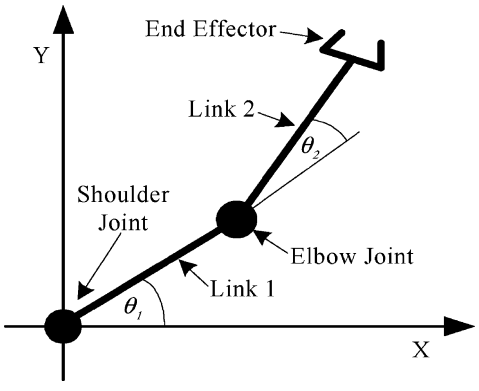

Fig. 1 Two-link flexible robot.

For a two-link robot M_r and C_r are given by

$$\boldsymbol{M}_r = \begin{bmatrix} \frac{1}{3}m_1L^2 + m_2L^2\left(\frac{4}{3} + \cos\theta_2\right) & m_2L^2\left(\frac{1}{3} + \frac{1}{2}\cos\theta_2\right) \\ m_2L^2\left(\frac{1}{3} + \frac{1}{2}\cos\theta_2\right) & \frac{1}{3}m_2L^2 \end{bmatrix} \tag{5}$$

$$\boldsymbol{C}_r = -\left(\frac{1}{2}m_2L^2\sin\theta_2\right)\begin{bmatrix} \dot{\theta}_2(2\dot{\theta}_1 + \dot{\theta}_2) \\ -\dot{\theta}_1 \end{bmatrix} \tag{6}$$

Flexible Dynamics

Modeling flexible robot dynamics with assumed modes of vibration for Euler–Bernoulli beam boundary conditions is a well-established technique. It captures the interaction between flexural vibrations and nonlinear rigid multibody dynamics such that a model can be derived to simulate the dynamic behavior of a flexible robot.[4,5,10–12] Extensive literature exists on the dynamics and control of flexible single- and two-link robots, of which the references cited are a select few on the use of assumed modes to model flexibility.[4,5,10–12] This approach accommodates changes in configuration during operation, whereas natural modes must be continually recomputed. Elastic deformations are modeled by a finite series of space-dependent, admissible functions, multiplied by a specific set of time-dependent amplitude functions, which result in amplitudes that form the generalized configuration coordinates in the Euler–Lagrange dynamics formulation. Admissible functions satisfy, at least, system geometric boundary conditions. A chosen set of admissible functions forms the basis functions in the assumed modes method and are applied to the robot throughout its operational workspace, provided geometric boundary conditions are consistent. Approximate deformation of any continuous elastic beam subjected to transverse vibrations is given by

$$u(x, t) = \sum_{i=1}^{n} \phi_i(x)q_i(t) \tag{7}$$

where $\phi_1(x)$ is the dominant assumed mode shape for specific beam boundary conditions. The shape function $u(x, t)$ substitutes into the Euler–Lagrange dynamics equations (1) and (2) (Refs. 4 and 10–12).

Mode Summation

In general, for an Euler–Bernoulli beam with uniform distributed load, the equation of motion is given by[13]

$$\frac{\partial^2}{\partial x^2}\left(EI\frac{\partial^2 u(x,t)}{\partial x^2}\right)\mathrm{d}x + m(x)\frac{\partial^2 u(x,t)}{\partial t^2} = p(x,t) \tag{8}$$

The normal modes ϕ_i must satisfy Eq. (9) and its boundary conditions:

$$(EI\phi_i'')'' - \omega_i^2 m(x)\phi_i = 0 \tag{9}$$

Its solution is given by Eq. (7).

For generalized elastic coordinates $q_i = q_1, \ldots, q_n$ the elastic kinetic and potential energies are given by

$$T_e = \frac{1}{2}\sum_{i}^{n}\sum_{j}^{n}\dot{q}_i\dot{q}_j\int_0^L \phi_i\phi_i m(x)\,\mathrm{d}x = \frac{1}{2}\sum_{i}^{n} M_i\dot{q}_i^2 \tag{10}$$

where

$$M_i = \int_0^L \phi_i^2(x)m(x)\,\mathrm{d}x$$

$$U_e = \frac{1}{2}\sum_{i}^{n}\sum_{j}^{n}\dot{q}_i\dot{q}_j\int_0^L EI\phi_i''\phi_i''\,\mathrm{d}x = \frac{1}{2}\sum_{i}^{n} K_i\dot{q}_i^2$$

$$= -\frac{1}{2}\sum_{i}^{n}\omega_i^2 M_i\dot{q}_i^2 \tag{11}$$

Combining flexible equations of motion with rigid-dynamics equations, we obtain a flexible-robot dynamics equation given by

$$\boldsymbol{\tau} = \boldsymbol{M}(\boldsymbol{q})\ddot{\boldsymbol{q}} + \boldsymbol{C}(\dot{\boldsymbol{q}}, \boldsymbol{q})\dot{\boldsymbol{q}} + \boldsymbol{K}\boldsymbol{q} \tag{12}$$

Matrix $\boldsymbol{M}$ comprises rigid and flexible link elements, $\boldsymbol{C}$ comprises rigid and elastic Coriolis and centrifugal effects, and $\boldsymbol{K}$ is a stiffness matrix. The generalized coordinate vector $\boldsymbol{q}$ comprises joint angles and flexible link deformations. In the calculation of the assumed modes of vibration, small elastic deformations is an underlying assumption, where second-order terms of interacting elastic modes can be neglected and, together with orthogonality properties of assumed modes, simplify Eq. (12). Omitting elastic Coriolis and centrifugal components for a two-link flexible robot gives a coupling matrix equal to $\boldsymbol{C}_r$ in Eqs. (4) and (6). Full dynamics equations for a multi-DOF manipulator has been derived previously.[14]

Cantilever and Pinned–Pinned Assumed Modes

From transverse beam vibration theory, cantilever mode shapes are given by[13,15]

$$\phi_{ci}(x) = \cosh\lambda_{ci}x - \cos\lambda_{ci}x - k_{ci}(\sinh\lambda_{ci}x - \sin\lambda_{ci}x) \tag{13}$$

where

$$k_{ci} = \frac{\cos\lambda_{ci}L + \cosh\lambda_{ci}L}{\sin\lambda_{ci}L + \sinh\lambda_{ci}L}$$

for which $\lambda_{ci}L \approx (i - \frac{1}{2})\pi$, $i = 1, \ldots, n$, are numerically approximated roots of the characteristic equation $\cos(\lambda_{ci}L)\cosh(\lambda_{ci}L) + 1 = 0$.

Modal frequencies are given by

$$\omega_{ci} = (\lambda_{ci}L)^2\sqrt{EI/\rho L^4} \tag{14}$$

Proportional and derivative gains for the dominant cantilever assumed mode frequency ω_{c1} are given by

$$\boldsymbol{K}_p = \mathrm{diag}\left[\omega_{c1}^2 \quad \omega_{c1}^2\right] = \mathrm{diag}[150.79,\ 150.79] \tag{15}$$

$$\boldsymbol{K}_d = \mathrm{diag}[2\zeta\omega_{c1} \quad 2\zeta\omega_{c1}] = \mathrm{diag}[17.364,\ 17.364] \tag{16}$$

for $\omega_{c1} = 12.28$ Hz.

Pinned–pinned mode shapes are given by[13,15]

$$\phi_{\mathrm{pp}i} = \sqrt{(2/\rho L)}\sin\lambda_{\mathrm{pp}i}x \tag{17}$$

for which $\lambda_{\mathrm{pp}i}L = i\pi$ are roots of the characteristic equation $\sin\lambda_{\mathrm{pp}i}L = 0$, $i = 1, \ldots, n$.

Modal frequencies are given by

$$\omega_{\mathrm{pp}i} = (\lambda_{\mathrm{pp}i}L)^2\sqrt{EI/\rho L^4} \tag{18}$$

For pinned–pinned assumed modes, the tip of a link coincides with that of a rigid link with angle θ_t subtended at the joint by the tip.[10]

Proportional and derivative gains for the dominant pinned–pinned assumed mode frequency $\omega_{\mathrm{pp}1}$ are given by

$$\boldsymbol{K}_p = \mathrm{diag}\left[\omega_{pp1}^2 \quad \omega_{\mathrm{pp}1}^2\right] = \mathrm{diag}[1188.4 \quad 1188.4] \tag{19}$$

$$\boldsymbol{K}_d = \mathrm{diag}[2\zeta\omega_{pp1} \quad 2\zeta\omega_{\mathrm{pp}1}] = \mathrm{diag}[48.746 \quad 48.746] \tag{20}$$

for $\omega_{\mathrm{pp}1} = 34.474$ Hz.

Control Law

An intuitive Jacobian transpose control law provides a joint actuating torque vector given by[3,4]

$$\boldsymbol{\tau} = \boldsymbol{J}^T(\theta)\left[\boldsymbol{K}_p\begin{pmatrix} e_x \\ e_y \end{pmatrix} + \boldsymbol{K}_d\begin{pmatrix} \dot{e}_x \\ \dot{e}_y \end{pmatrix}\right] \tag{21}$$

Commanded x_c, and y_c positions for the desired trajectory input to the control system and sum with negative feedback actual position values to form position and velocity errors then are operated on by proportional and derivative gains, $\boldsymbol{K}_p$ and $\boldsymbol{K}_d$, to compute the Jacobian transpose control law. The damping ratio $\zeta = 0.707$ is estimated.

Control Strategy

A block diagram of the nonadaptive control strategy shown in Fig. 2 comprises a proportional derivative feedback loop with an inverse dynamics inner loop. When Eq. (21) is used, torque actuating each joint feeds into the inverse flexible dynamics equations to give an angular acceleration vector, which is double integrated to obtain joint rates and slew angles. Slew angles θ_1 and θ_2 together with flexural deformations δ_1 and δ_2 feed back into the inverse dynamics equations. Slew angles also transform into x and y endpoint positions in the direct kinematics Eqs. (22) and (23) and feed back to form position errors $e_x = x_c - x$ and $e_y = y_c - y$. Slew rates $\dot{\theta}_1$ and $\dot{\theta}_2$ feed back to form velocity errors $\dot{e}_x = \dot{x}_c - \dot{x}$ and $\dot{e}_y = \dot{y}_c - \dot{y}$:

$$x = L_1\cos(\theta_1) + L_2\cos(\theta_1 + \theta_2) \tag{22}$$

$$y = L_1\sin(\theta_1) + L_2\sin(\theta_1 + \theta_2) \tag{23}$$

Fuzzy Logic System

Figure 3 shows the fuzzy adaptive control strategy with a fuzzy logic system (FLS) included. The FLS is a Mamdani type, and each variable is designed with nine Gaussian membership functions.[3,8] Verbal descriptors for positive maximum (PMAX), positive very very high (PVVH), positive very high (PVH), positive high (PH), positive medium (PM), positive low (PL), positive very low (PVL), positive very very low (PVVL), zero (ZERO), negative very high (NVH), negative high (NH), negative medium (NM), negative low (NL), and negative very low (NVL) are used in generating fuzzy rules typically of the form

IF δ_1 is NL AND δ_2 is PL THEN λ is PM

IF δ_1 is PVL AND δ_2 is PVH THEN λ is PH

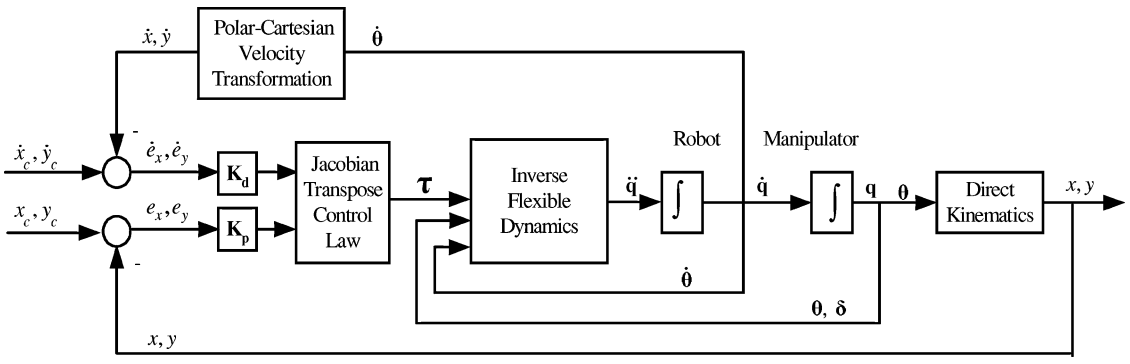

Fig. 2 Nonadaptive control strategy.

Table 1 Fuzzy logic system rule matrix

		δ_2								
	λ	NVH	NH	NL	NVL	ZERO	PVL	PL	PH	PVH
	NVH	PMAX	PVVH	PVH	PH	PM	PH	PVH	PVVH	PMAX
	NH	PVVH	PVH	PH	PM	PL	PM	PH	PVH	PVVH
	NL	PVH	PH	PM	PL	PVL	PL	PM	PH	PVH
	NVL	PH	PM	PL	PVL	PVVL	PVL	PL	PM	PH
δ_1	ZERO	PM	PL	PVL	PVVL	ZERO	PVVL	PVL	PL	PM
	PVL	PH	PM	PL	PVL	PVVL	PVL	PL	PM	PH
	PL	PVH	PH	PM	PL	PVL	PL	PM	PH	PVH
	PH	PVVH	PVH	PH	PM	PL	PM	PH	PVH	PVVH
	PVH	PMAX	PVVH	PVH	PH	PM	PH	PVH	PVVH	PMAX

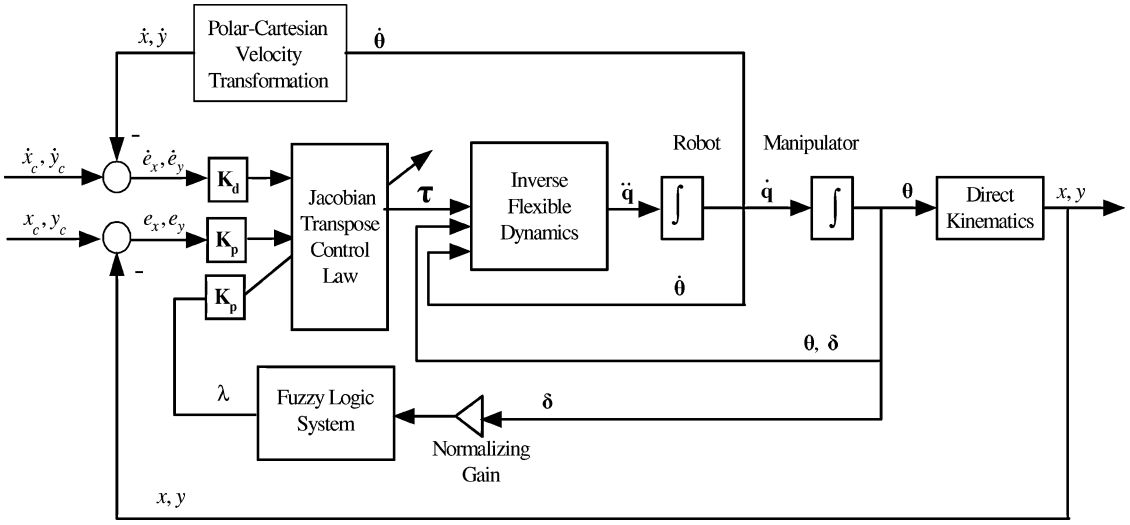

Fig. 3 Fuzzy adaptive control strategy.

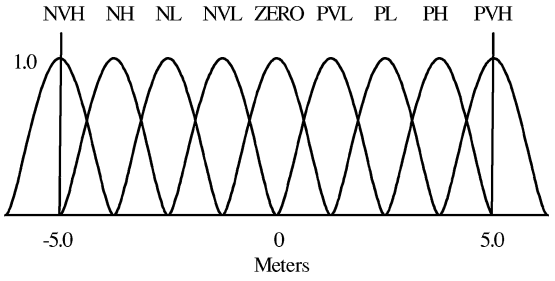

Fig. 4 Membership functions for input variables δ_1 and δ_2.

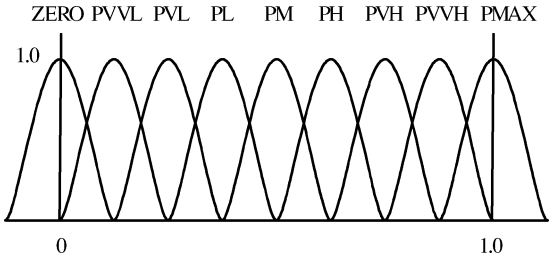

Fig. 5 Membership functions for output variable λ.

Figures 4 and 5 show the FLS membership functions for elastic-link deformation input variables δ_1 and δ_2 and output variable λ. Universes of discourse range from −5 to 5 m for δ_1 and δ_2 and from 0 to 1 for λ. The FLS is developed intuitively, such that, as the magnitude of elastic deformation for each link varies positively or negatively, it complements or counters deformation of the other link. The value of λ varies according to the magnitude of resultant deformation and is maintained at $\lambda > 0$ ranging from ZERO for zero deformation to PMAX for the largest deformation, thereby forming the symmetric fuzzy rule matrix given in Table 1.

Within the FLS, antecedent composition, implication, aggregation, and defuzzification methods are MIN, MIN, MAX, and CENTROID, respectively. Crisp values of δ_1 and δ_2 input to the FLS fuzzify to produce a degree of membership $0 <= \mu <= 1$. The MIN operator determines the minimum value of μ causing the implication operator MIN to truncate the output membership function. The MAX operator aggregates all truncated output membership functions resulting in a composite membership function. This aggregate is defuzzified using the CENTROID method. The CENTROID method calculates the center of area (COA) of the aggregate membership function and results in a μ value corresponding to a crisp value for λ, given by[2,3,7,8]

$$\mathrm{COA} = \frac{\int \mu(\lambda)\lambda \, \mathrm{d}\lambda}{\int \mu(\lambda) \, \mathrm{d}\lambda} \tag{24}$$

Scaling gain K_s multiplies output variable λ fuzzy membership functions to modify their base widths and provide greater tracking accuracy toward asymptotically zero position errors as K_s increases. The achievement of good results with a suitable K_s value necessitated experimentation by performing simulations with iterations for unit increments of K_s up to 50. Initial results for $K_s = 1$ demonstrated poor tracking control similar to the nonadaptive results shown in Figs. 6 and 7 but then gradually improved for each successive iteration until the trajectories shown in Figs. 8 and 9 were achieved using $K_s = 50$. Adaptive control is achieved by adapting the Jacobian transpose control law with λ multiplied by scaling gain K_s. The adaptive control law is given by

$$\boldsymbol{\tau} = \boldsymbol{K}_s \lambda \left\{ \boldsymbol{J}^T(\theta) \left[\boldsymbol{K}_p \begin{pmatrix} e_x \\ e_y \end{pmatrix} + \boldsymbol{K}_d \begin{pmatrix} \dot{e}_x \\ \dot{e}_y \end{pmatrix} \right] \right\} \tag{25}$$

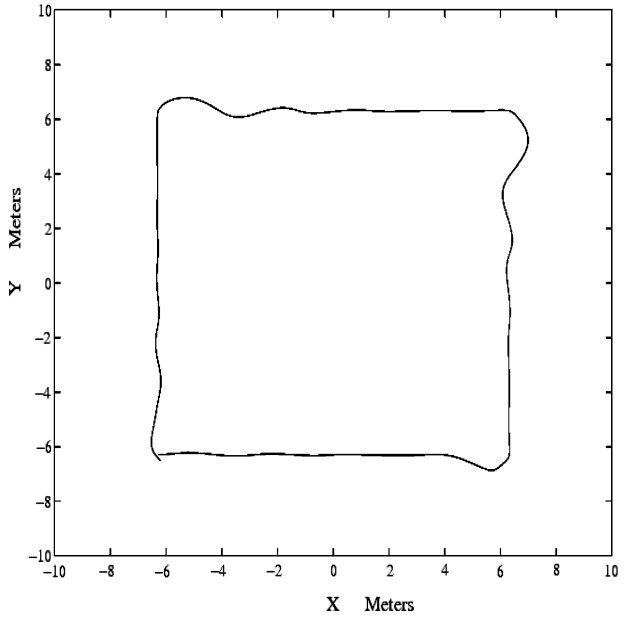

Fig. 6 Cantilever nonadaptive tracking.

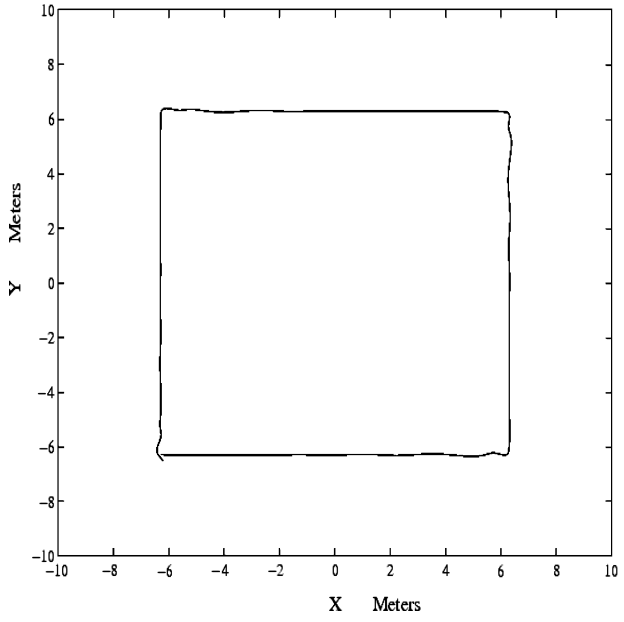

Fig. 7 Pinned–pinned nonadaptive tracking.

Simulation Results

Figures 6–9 show the results of tracking endpoint trajectories in a clockwise direction starting at the lower-left-hand corner. For the nonadaptive cantilever model shown in Fig. 6, pronounced overshoots occur at each direction switch caused by flexibility. However, the trajectory for the fuzzy adaptive cantilever model shown in Fig. 8 exhibits minimal overshoots and rapid settling to a steady state. Minimal overshoots occur at direction switches for the nonadaptive pinned–pinned model trajectory shown in Fig. 7. These are greatly diminished by adaptive control using the FLS and provide asymptotically zero errors such that tracking is close to a straight line along each side of the trajectory shown in Fig. 9. Link deformations and the corresponding values of λ are shown in Figs. 10 and 11 for the adaptive cantilever mode model. Deformations are initially low, at $+0.1/-0.08$ and $+0.03/-0.035$ m for links 1 and 2, respectively, then gradually decrease to $+0.04/-0.03$ and $+0.01/-0.025$ m along the first side of the trajectory but sharply increase to $+0.17/-0.15$ and $+0.075/-0.08$ m for links 1 and 2, respectively, as a result of the disturbance at the first direction switch. Thereafter,

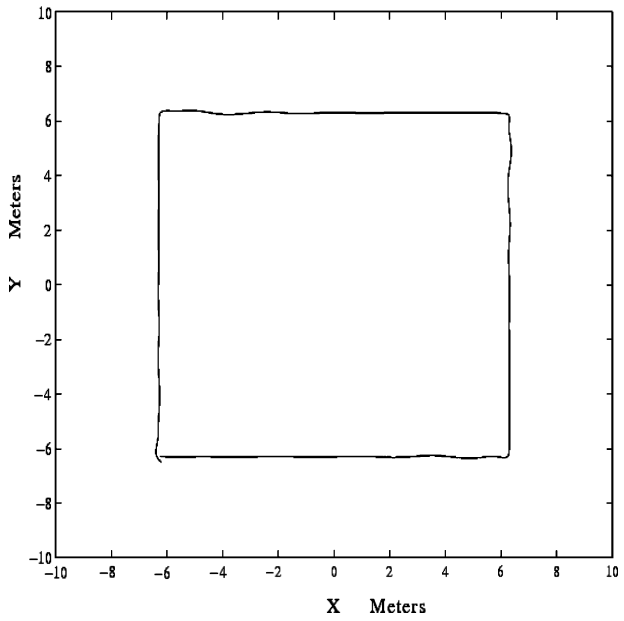

Fig. 8 Cantilever fuzzy adaptive tracking.

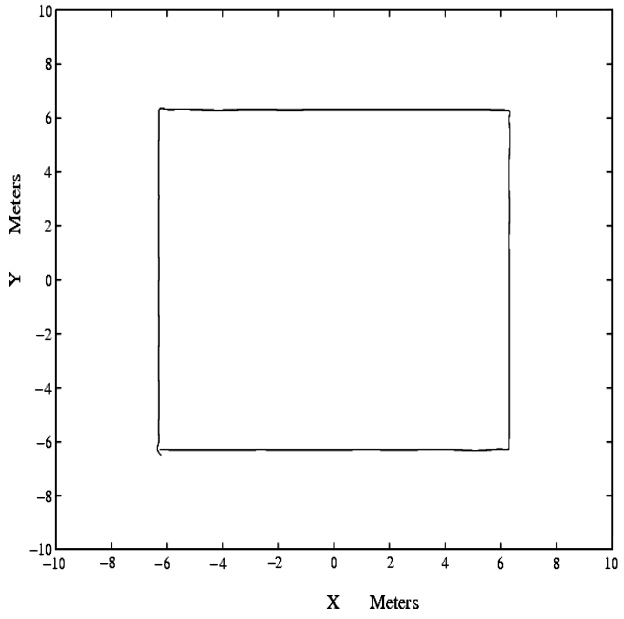

Fig. 9 Pinned–pinned fuzzy adaptive tracking.

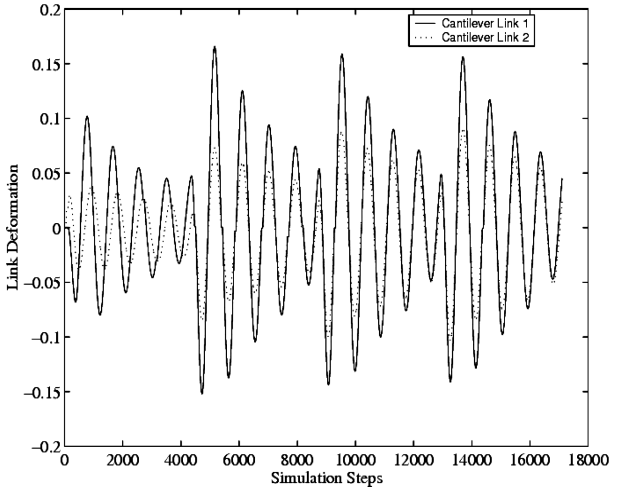

Fig. 10 Link deformations δ_1 and δ_2 for cantilever robot dynamics model.

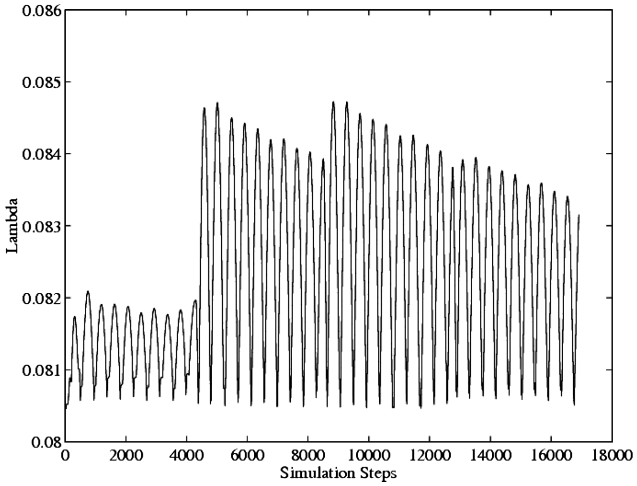

Fig. 11 Output variable λ for cantilever link deformations δ_1 and δ_2.

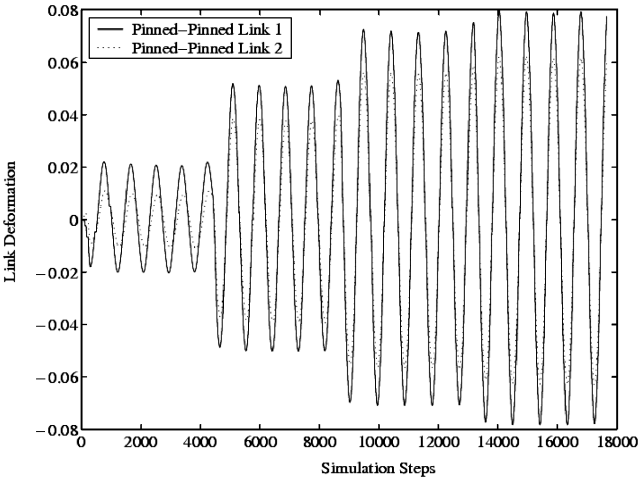

Fig. 12 Link deformations δ_1 and δ_2 for pinned–pinned robot dynamics model.

deformation magnitudes diminish gradually to +0.05/−0.055 and +0.025/0.04 m but again sharply increase to +0.17/−0.15 and +0.085/−0.1 m for links 1 and 2, respectively, caused by oscillations excited at the subsequent second and third direction switches followed by the same diminishing oscillations sequence. Corresponding λ values, shown in Fig. 11, are relatively low, averaging 0.0813, and peak at 0.082 along the first side of the trajectory, then increase to average 0.0825 and peak at 0.0847 at the first and second direction switches, and then average 0.0821 and peak at 0.084 at the third direction switch, adapting the control law to provide reduction of the vibration amplitudes. The peak values of λ gradually decrease after each direction switch as the adaptive control law takes effect. Deformations for the adaptive pinned–pinned model, shown in Fig. 12, are initially low, at ±0.02 and ±0.01 m for links 1 and 2, respectively, along the first side of the trajectory and then increase sharply to ±0.05 and ±0.036 m for links 1 and 2, respectively, at the first direction switch. Subsequently, deformations sharply increase to ±0.07 and ±0.055 m at the second direction switch and then to ±0.08 and ±0.06 m at the third direction switch for links 1 and 2, respectively. Corresponding λ values, shown in Fig. 13, are relatively low, averaging 0.0815, and peak at 0.082 along the first side of the trajectory, then increase to average 0.084 and peak at 0.086 at the first direction switch, and then average 0.085 and peak at 0.089 at the second and average 0.0855 and peak at 0.09 at the third direction switches adapting the control law to provide reduction of the vibration amplitudes. The results demonstrate an anomaly of the pinned–pinned model to increase oscillations after

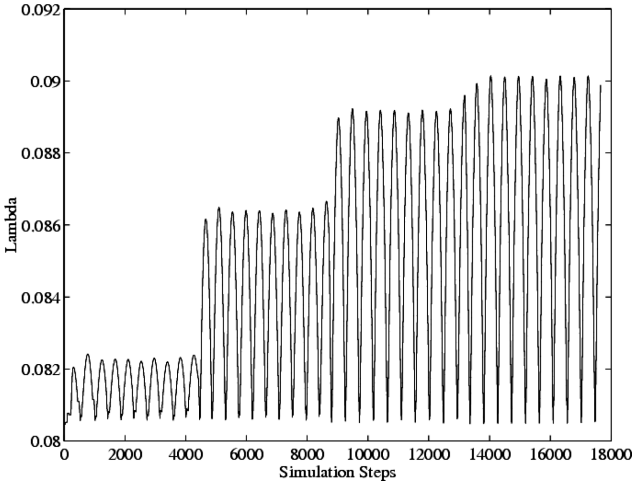

Fig. 13 Output variable λ for pinned–pinned link deformations δ_1 and δ_2.

each disturbance, requiring progressively higher λ values to control them because of zero restraining forces and moments at the boundary conditions, whereas cantilever model oscillations diminish, requiring progressively lower λ values after each disturbance as a result of the restoring force and moment at the fixed-end boundary condition.

Simulation times were 11 min 28 s for cantilever and 11 min 45 s for pinned–pinned models with nonadaptive control and 26 min 33 s for cantilever and 27 min 55 s for pinned–pinned models with fuzzy adaptive control, respectively.[16] Other researchers use an experimental two-link flexible space robot to track a 75-cm square trajectory in 40 s with a series steady-state linear quadratic regulator control technique. Their results do not compare favorably with results presented in this paper.[6] However, results obtained by others tracking a square trajectory with a two-link flexible robot and an input shaping control technique do compare closely to the results given in this paper.[1] Control Systems and Fuzzy Logic Toolboxes were used for all simulations.

Conclusions

This paper endorses established theory for coupling large rotations with assumed small flexural deformations in deriving the Euler–Lagrange flexible dynamics equations to characterize a two-link flexible robot. The complexities of flexible dynamics and poor control by classical methods are overcome by implementing an FLS to produce an output variable in response to elastic deformations of the links and to adapt the Jacobian transpose control law so that tracking errors are reduced. Modes of vibration are determined by assuming geometric boundary conditions of the robot consistent for configuration changes in its operational workspace. In this study, the dominant mode is used to derive flexible dynamics models for cantilever and pinned–pinned boundary conditions. Initially, imprecise tracking results are obtained using a nonadaptive control strategy, and then greatly improved tracking results are achieved using an adaptive control strategy with an FLS. The FLS is effective for both cantilever and pinned–pinned models but more significantly for the cantilever model. However, these results are obtained at a high computational time burden for both robot models. The results are representative of multi-DOF systems, and the adaptive control strategy can be extended to a broad range of applications. Future work could investigate adaptation of control laws for flexible dynamics models with higher modes.

References

[1]Banerjee, A. K., and Singhose, W., "Command Shaping in Tracking Control of a Two-Link Flexible Robot," *Journal of Guidance, Control, and Dynamics*, Vol. 21, No. 6, 1998, pp. 1012–1015.

[2]de Silva, C. W., *Intelligent Control: Fuzzy Logic Applications*, CRC Press, Boca Raton, FL, 1995, pp. 173–209.

[3]Green, A., and Sasiadek, J. Z., "Methods of Trajectory Tracking for Flexible Manipulators," AIAA Paper 2002-4565, Aug. 2002.

[4]Green, A., and Sasiadek, J. Z., "Robot Manipulator Control for Rigid and Assumed Mode Flexible Dynamics Models," AIAA Paper 2003-5435, Aug. 2003.

[5]Sasiadek, J. Z., and Srinivasan, R., "Dynamic Modeling and Adaptive Control of a Single-Link Flexible Manipulator," *Journal of Guidance, Control, and Dynamics*, Vol. 12, No. 6, 1989, pp. 838–844.

[6]Carusone, J., Buchan, K. S., and D'Eleuterio, G. M. T., "Experiments in End-Effector Tracking Control for Structurally Flexible Space Manipulators," *IEEE Transactions on Robotics and Automation*, Vol. 9, No. 5, 1993, pp. 553–560.

[7]Lee, J. X., Vukovich, G., and Sasiadek, J. Z., "Fuzzy Control of a Flexible Link Manipulator," *Proceedings of the American Control Conference*, WM7-1:50, Omnipress, Madison, WI, 1994, pp. 568–574.

[8]Passino, K. M., and Yurkovich, S., *Fuzzy Control*, Addison–Wesley, Menlo Park, CA, 1990, pp. 116–132.

[9]Asada, H., and Slotine, J.-J. E., *Robot Analysis and Control*, Wiley, New York, 1986, pp. 104–118.

[10]Fraser, A. R., and Daniel, R. W., *Perturbation Techniques for Flexible Manipulators*, Kluwer International Series in Engineering and Computer Science, Vol. 138, Kluwer, Dordrecht, The Netherlands, 1991, pp. 170–173.

[11]Junkins, J. L., and Kim, Y., *Introduction to Dynamics and Control of Flexible Structures*, edited by J. S. Przemieniecki, AIAA Education Series, AIAA, Washington, DC, 1993, pp. 139–234.

[12]Mordfin, T. G., and Tadikonda, S. S. K., "Truth Models for Articulating Flexible Multibody Dynamic Systems," *Journal of Guidance, Control, and Dynamics*, Vol. 23, No. 5, 2000, pp. 805–811.

[13]Thomson, W. T., *Theory of Vibration with Applications*, 2nd ed, Prentice–Hall, Upper Saddle River, NJ, 1981, pp. 218–221, 238–256, 340–345.

[14]Beres, W., and Sasiadek, J. Z., "Finite Element Dynamic Model of Multi-Link Flexible Manipulators," *Applied Mathematics and Computer Science*, Vol. 5, No. 2, 1995, pp. 231–262.

[15]Timoshenko, S., Young, D. H., and Weaver, W., Jr., *Vibration Problems in Engineering*, 4th ed, Wiley, New York, 1974, pp. 415–431.

[16]"Matlab 6, Simulink 4, Control Systems and Fuzzy Logic Toolboxes," Release 12, MathWorks, Natick, MA, 2001.